THE JOURNAL OF PHYSICAL CHEMISTRY Letters

Letter

pubs.acs.org/JPCL

Intercalated vs Nonintercalated Morphologies in Donor–Acceptor Bulk Heterojunction Solar Cells: PBTTT:Fullerene Charge Generation and Recombination Revisited

Elisa Collado-Fregoso,[†,∥] Samantha N. Hood,[‡] Safa Shoaee,[†] Bob C. Schroeder,[§,∥] Iain McCulloch,[∥,⊥] Ivan Kassal,[‡,#] Dieter Neher,*[,†] and James R. Durrant*[,∥,▽]

[†]Department of Physics and Astronomy, University of Potsdam, Karl-Liebknecht-Straße 24–25, 14476 Potsdam-Golm, Germany

[‡]Centre for Engineered Quantum Systems, School of Mathematics and Physics, The University of Queensland, Brisbane, Queensland 4072, Australia

[§]Materials Research Institute and School of Biological and Chemical Sciences, Queen Mary University of London, Mile End Road, London E1 4NS, United Kingdom

[∥]Centre for Plastic Electronics, Department of Chemistry, Imperial College London, Exhibition Road, London SW7 2AZ, United Kingdom

[⊥]KSC, King Abdullah University of Science and Technology, Thuwal 23955-6900, Saudi Arabia

[#]Centre for Engineered Quantum Systems, Australian Institute for Nanoscale Science and Technology, and School of Chemistry, The University of Sydney, Sydney, New South Wales 2006, Australia

[▽]SPECIFIC IKC, College of Engineering, Swansea University, Swansea SA12 7AX, United Kingdom

Supporting Information

ABSTRACT: In this Letter, we study the role of the donor:acceptor interface nanostructure upon charge separation and recombination in organic photovoltaic devices and blend films, using mixtures of PBTTT and two different fullerene derivatives ($PC_{70}BM$ and ICTA) as models for intercalated and nonintercalated morphologies, respectively. Thermodynamic simulations show that while the completely intercalated system exhibits a large free-energy barrier for charge separation, this barrier is significantly lower in the nonintercalated system and almost vanishes when energetic disorder is included in the model. Despite these differences, both femtosecond-resolved transient absorption spectroscopy (TAS) and time-delayed collection field (TDCF) exhibit extensive first-order losses in both systems, suggesting that geminate pairs are the primary product of photoexcitation. In contrast, the system that comprises a combination of fully intercalated polymer:fullerene areas and fullerene-aggregated domains (1:4 PBTTT:$PC_{70}BM$) is the only one that shows slow, second-order recombination of free charges, resulting in devices with an overall higher short-circuit current and fill factor. This study therefore provides a novel consideration of the role of the interfacial nanostructure and the nature of bound charges and their impact upon charge generation and recombination.

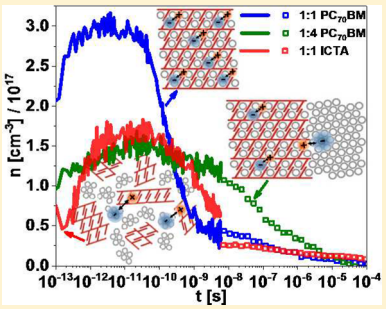

The charge separation process in organic photovoltaic blends has long been studied; however, significant discrepancies remain on proposed mechanisms of free polaron generation.[1−3] Variables often cited as influencing the yield of free charges are the driving energy for charge separation,[4,5] the availability of excited states that support a large electron delocalization,[6−9] the dielectric constant of the blend,[10] and the mobility of the photogenerated charges.[11] All of these factors are related to the micro- and nanostructure of the blend, namely, the crystallinity, domain size, and purity of the blend components.[12−18] More recently, the orientation of the donor and acceptor molecules with respect to each other has been proposed as a critical nanostructure parameter,[18,19] and the polarization energy at the interface has been suggested to affect the charge separation energy barrier.[20]

It is generally accepted that a trade-off exists between the optimal microstructure for efficient exciton dissociation and that for efficient separation of the charges and their subsequent collection.[21] While molecularly intermixed regions of donor and acceptor are thought to be optimal for exciton dissociation, more pure, extended regions of either component have proven necessary for efficient charge separation and collection.[13,21−25] In addition, the nature of the morphological distribution in the donor–acceptor interface, whether blurred with a continuous composition gradient or presenting an abrupt transition between the donor and acceptor phase, was predicted to affect the efficiency of exciton harvesting and charge extraction, thus

Received: June 20, 2017
Accepted: August 4, 2017
Published: August 4, 2017

DOI: 10.1021/acs.jpclett.7b01571
J. Phys. Chem. Lett. 2017, 8, 4061−4068

impacting the overall device performance.[23,26,27] A key uncertainty in such analyses is the nature of the interfacial bound charges in such bulk heterojunction (BHJ) devices and their impact upon charge generation and recombination.

In this Letter, we provide a combined experimental and theoretical study of the role of the interface nanostructure upon charge separation and recombination energetics and kinetics. We show, for the first time, that charge recombination kinetics at times that cover 10 orders of magnitude, obtained from all-optical (fs-transient absorption spectroscopy (TAS) and photoluminescence (PL) in blends) and electro-optical techniques (time-delayed collection field (TDCF) in devices), agree with each other in systems with efficient charge separation. Our study employs the prototypical polymer PBTTT (poly[2,5-bis(3-tetradecylthiophen-2-yl)thieno[3,2-*b*]-thiophene] blended with different loadings of $PC_{70}BM$ ([6,6]-phenyl C71 butyric acid methyl ester) and with a bulky acceptor, ICTA (indene-C60 trisadduct; see the chemical structures and UV−vis of the neat and blend films used herein in Figure S1). The critical difference between these blends is that they give rise to very particular interfacial nanostructures.[28−31] The 1:1 PBTTT:$PC_{70}BM$ blend comprises fully intermixed polymer:fullerene co-crystals with a molecular interface; this system will be referred here as "intercalated". The 1:1 PBTTT:ICTA blend does not show intercalation and has an abrupt interface; this system will be referred to as "nonintercalated". Finally, the 1:4 PBTTT:$PC_{70}BM$ blend presents both intercalated polymer:fullerene co-crystals and pure fullerene phases and herein will be referred to as "composite".[28−31]

We find from our simulations that the free energy of charge separation monotonically increases with increasing electron−hole distance when the PBTTT:$PC_{70}BM$ co-crystal is the predominant microstructure, meaning that photogenerated charges are unlikely to spontaneously separate at room temperature. However, this barrier is largely reduced for a nonintercalated sharp donor−acceptor interface such as the one present in PBTTT:ICTA and almost vanishes if energetic disorder is included in the model. In agreement with this theory, TDCF studies reveal a pronounced electric field dependence of charge generation in the PBTTT:$PC_{70}BM$ co-crystal but not in the phase-separated PBTTT:ICTA blend. Surprisingly, photovoltaic devices fabricated with the latter blend perform worst among all systems studied. Our TAS and TDCF recombination studies suggest that the nonintercalated blend suffers from delayed first-order recombination, which is consistent with the trapped charges in small and isolated PBTTT and/or ICTA domains. Importantly, geminate recombination is avoided in the composite system, the only system that comprises a combination of intercalated and pure fullerene phases. Therefore, our study highlights the importance of multiphase morphology when aiming for efficient generation and extraction of charge in BHJ solar cells.

First, we confirm the nanostructure of the active blends. Figure 1 shows wide-angle X-ray diffraction (WAXD) results in films of neat PBTTT and blends of PBTTT:fullerene, where it can be observed that rather large crystallites are formed in both the neat and blend films, ranging between 7 and 13 nm (see Table S1 for details on crystallite sizes). In the 1:1 and 1:4 PBTTT:$PC_{70}BM$, the lamellar peaks shift to q = 0.217 and 0.218 $Å^{-1}$, corresponding to lamellar spacings of 29.0 and 28.8 Å, respectively, compared to the 20.6 Å spacing in the neat PBTTT film fabricated with the same conditions. Conversely,

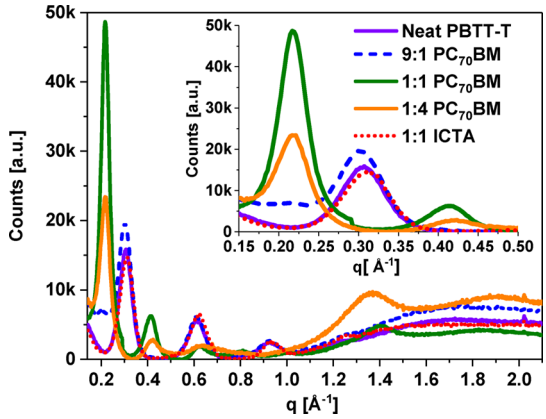

Figure 1. WAXD of neat PBTTT and PBTTT:fullerene thin films with different fullerene loadings.

for the nonintercalated systems, the peak remains at q = 0.309 $Å^{-1}$, corresponding to a lamellar spacing of 20.3 Å, very close to the lamellar spacing in the neat PBTTT film. This confirms, as previously reported, that the system that contains a sufficient amount of a small fullerene, such as the 1:1 blend with $PC_{70}BM$, shows predominant intercalation.[28−31] This blend thus constitutes an ideal model system for a blend with only molecular heterojunctions, where every donor molecule neighbors an acceptor and vice versa. In contrast, the ICTA blend does not intercalate and therefore constitutes a model of an abrupt interface between pure phases, which we denote as a domain heterojunction. We have further confirmed these results using resonant Raman spectroscopy.[32]

In order to assess how the nature of the heterojunction affects the efficiency of charge generation, we performed simulations of the free energy $\Delta G(r)$ of the electron−hole pair. As we have previously described,[33] the electron and hole are initially simulated as a charge-transfer (CT) state with the hole in the PBTTT and the electron in the acceptor ($PC_{70}BM$ or ICTA).[33−35] The free energy $\Delta G(r)$ of the electron−hole pair as a function of their separation r is then calculated with and without energetic disorder. For the intercalated case, the PBTTT:$PC_{70}BM$ mixture is modeled as one phase with both the donor and acceptor forming one-dimensional channels, according to previous literature reports.[30,36] For the non-intercalated case, the morphology was represented as two phases of a three-dimensional hexagonal close-packed lattice with a planar interface between them. Additional simulation details are described in section 2 of the SI, including Figures S2 and S3, which show a schematic representation of the two cases.

Figure 2 shows the results of these simulations. In the intercalated case, neither entropy nor disorder has a significant effect on the free energy of dissociation. In particular, there is no entropic driving because the number of accessible states does not increase with electron−hole separation when both carriers are confined to the one-dimensional channels formed in the intercalated blend.[35] Conversely, for the nonintercalated case, entropy and disorder decisively lower the energetic barrier for charge pair separation. The entropic driving comes from the fact that the number of ways of arranging two charges goes as the cube of their separation,[33] lowering the free energy. Energetic disorder also lowers the barrier by allowing charges on higher-energy sites to lower their energy by moving onto neighboring lower-lying sites, a process that is more likely to

DOI: 10.1021/acs.jpclett.7b01571
J. Phys. Chem. Lett. 2017, 8, 4061−4068

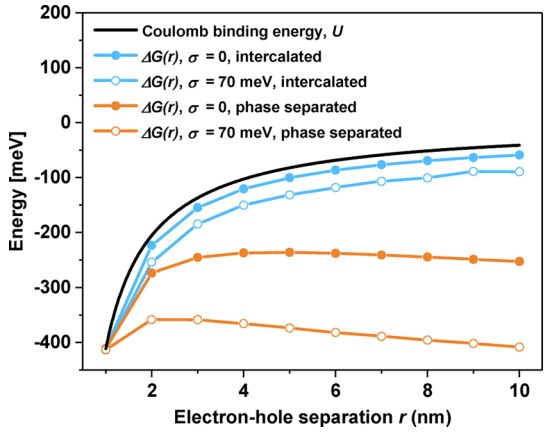

Figure 2. Electron−hole Coulombic binding (black curve) and free energy calculated without (σ = 0) and with 70 meV of Gaussian energetic disorder for a completely intercalated morphology (full circles) and for a phase-separated system (empty circles).

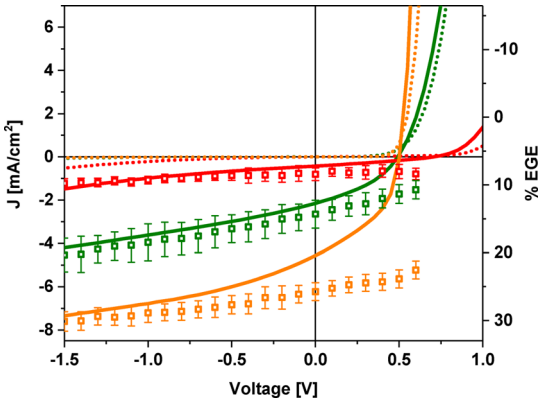

Figure 3. $J-V$ curves of representative, BHJ devices (ITO/PEDOT:PSS/active blend/Ca/Al) under a constant, 100 mW cm^{-2}, AM 1.5 spectrum from solar simulated light at room temperature. The active blends are composed of (w/w) 1:4 PBTTT:PC$_{70}$BM (orange curve), 1:1 PBTTT:PC$_{70}$BM (green curve), and 1:1 PBTTT:ICTA (red curve). Dotted lines correspond to the dark currents of the corresponding devices. Open squares represent the EGE as obtained by TDCF at 6 ns and using −2.5 V for the collection bias after excitation at 540 nm and 0.2 μJ cm^{-2} (see text).

occur in higher-dimensional systems where each site has more neighbors. In particular, we notice that using 70 meV of energetic disorder, a value estimated via photo-CELIV for another nonintercalated system, PBTTT:bis-PC$_{60}$BM,[37] is enough to lower the charge separation barrier to ∼50 meV. This is a much lower energetic barrier compared to the barrier of more than 250 meV calculated for the intercalated case, independent of the presence of energetic disorder. This would suggest that charge separation is energetically more favorable in a phase-separated system with a more abrupt interface. We emphasize, however, that even with a small energetic barrier, charge separation need not be 100% efficient because it is governed by kinetic properties that cannot be predicted from thermodynamic considerations; in particular, recombination could still be fast in phase-separated blends, leading to low efficiencies.

To determine whether the predominance of nonintercalated blends results in superior device performance, charge generation and recombination were studied in detail with a combination of different steady-state and transient methods. Figure 3 shows the $J-V$ curves of the PBTTT:fullerene devices (see the device parameters in Table S5) along with the external generation efficiency (EGE) obtained from our TDCF measurements, described elsewhere.[38,39] Briefly, a 3.8 ns monochromatic (here 532 nm) light pulse was shined into the device pixel while the device was held at a certain bias ("prebias" V_{pre}); after a certain delay time, the charges were extracted using a strong reverse bias ("collection bias" V_{coll}). The EGE was calculated as the ratio of the total charge carrier collected per photons shined. Data in Figure 3 were obtained by keeping the delay constant at the earliest time (6 ns) and lowest measurable intensity (0.2 μJ cm^2) while the prebias was changed, using a collection bias of $V_{coll} = -2.5V$.

As can be observed, the $J-V$ curves are well described (both in shape and absolute current) by our estimated EGE at reverse bias, where nongeminate charge recombination is reduced by the effect of the applied field. This means that the device photocurrent is generated exactly with the charges measured by TDCF at short delay times. It is also evident that, whereas for the intercalated device the effect of prebias on generation is relatively large (EGE decreases by 45% from −1.5 to 0.6 V), this effect is much less pronounced for the composite device (23%) and slightly less for the nonintercalated device (20%). The trend for the extreme cases, that is, intercalated vs nonintercalated, is in agreement with conclusions from earlier TDCF measurements on a similar system.[40] Consistent with our simulations, this finding suggests that free charge photogeneration in the intercalated 1:1 PBTTT:PC$_{70}$BM device proceeds via Coulombically bound intermediates (namely, charge pairs) that are bias-susceptible and extractable under strong applied bias. Conversely, the presence of relatively pure phases in the nonintercalated and composite devices results in charge separation significantly less dependent on the electric field, indicating a lower barrier for free charge formation in both systems. This is due to the formation of less bound charges or the formation of bound charges that are less bias-susceptible. Later on, we will see that the last explanation seems to fit well with the evidence obtained by other measurements for the nonintercalated, PBTTT:ICTA device.

Despite the low bias influence on the EGE for the nonintercalated device, it is striking how low the absolute EGE is even at a −1.5 V reverse bias and how poorly this device performs, given the thermodynamic prediction of suppressed geminate recombination at an abrupt domain heterojunction interface. To understand this apparent disagreement, we studied charge recombination dynamics, employing both fs-TAS and TDCF as a function of delay time. Although there have been several spectroscopic studies of PBTTT systems varying the amount of intermixed regions,[22,31,41−45] a detailed analysis of charge kinetics in both blends and working solar devices where the interfacial nanostructure is controlled has been lacking.

Figure S4 shows the fs-TAS spectra and kinetics of a neat PBTTT film and a 9:1 PBTTT:PC$_{70}$BM blend film. From these data, the singlet exciton photoinduced absorption band, with a maximum at ∼1250 nm, can be identified.[22] Its lifetime is estimated (at low intensity) to be τ = 146 ± 20 ps, consistent with the lifetime of other conjugated polymers used in organic photovoltaics.[46] The band that appears from ∼850 to 1050 nm for the 9:1 blend can be assigned to the photoinduced absorption of bound/free positive polarons in the polymer phase, consistent with other reports.[22,42,44,45] These are the

DOI: 10.1021/acs.jpclett.7b01571
J. Phys. Chem. Lett. 2017, 8, 4061−4068

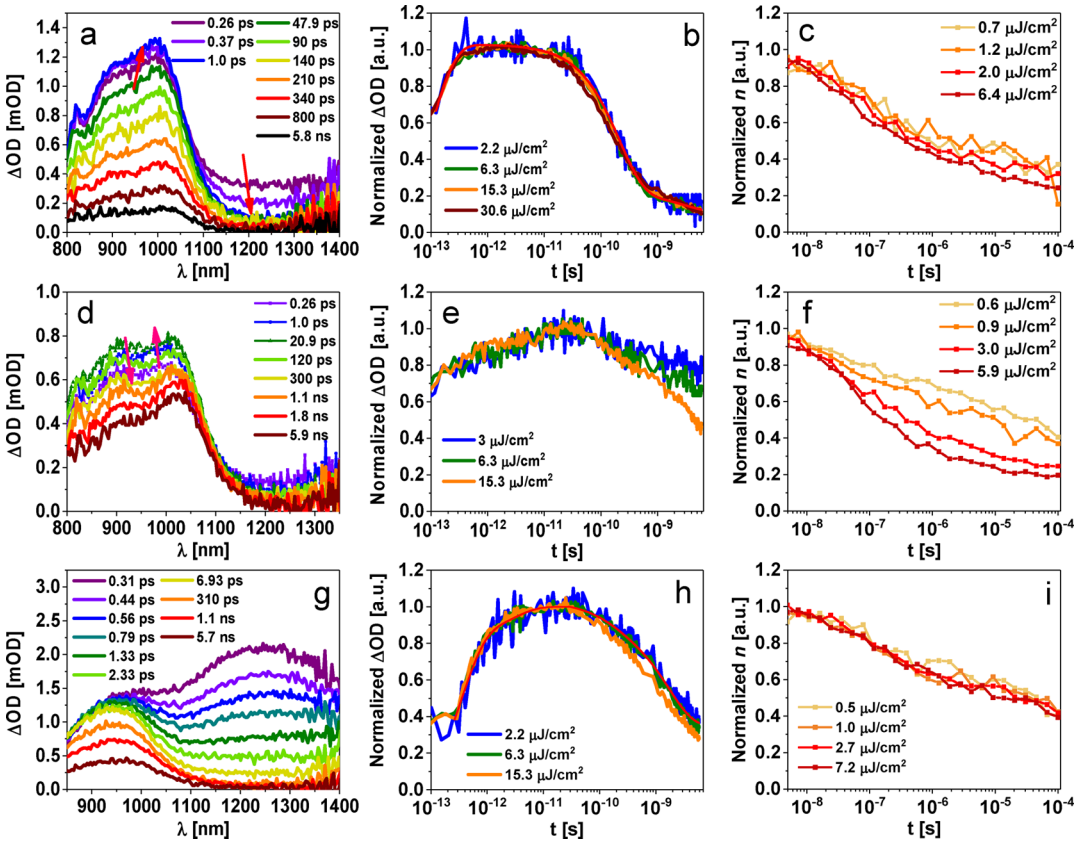

Figure 4. Three studied systems, one in each row: (a,b,c) 1:1 PBTTT:$PC_{70}BM$ (intercalated), (d,e,f) 1:4 PBTTT:$PC_{70}BM$ (composite), and (g,h,i) 1:1 PBTTT:ICTA (nonintercalated). Columns show (a,d,g) plots of TAS excited at 540 nm with 6 $\mu J/cm^2$, (b,e,h) normalized polaron recombination kinetics from TAS at the polaron absorption maximum, at different excitation intensities, and (c,f,i) normalized charge density from TDCF measurements at 0.4 V prebias and different light pulse intensities. Red lines in plots (b) and (h) correspond to triexponential fits of the data. Plot (g) shows the raw TAS spectra before subtracting exciton photoinduced absorption, which is included in the SI. Plot (h) shows deconvoluted polaron kinetics (the exciton contribution has been subtracted). See Table S4 for details of the fits.

basis of the assignments that will be used for the rest of the blends herein presented.

We now turn to Figure 4. Here we show, in the left column, the transient spectra of the blend films. The middle column shows the normalized TAS kinetics at the maximum of the bound/free polaron pairs (~1000 nm for the $PC_{70}BM$ blends and 930 nm for the ICTA blend), and the right one shows the corresponding normalized kinetics of total charge density obtained by TDCF at V_{pre} = 0.4 V (near V_{OC}). As is evident in panels (a) and (d) for the 1:1 and 1:4 PBTTT:$PC_{70}BM$ blends, the exciton photoinduced absorption band is scarcely present, indicating that exciton dissociation occurs on ultrafast time scales (≤200 fs), in agreement with previous studies[22,42,44,45] and consistent with the presence of completely intercalated areas. We note, however, that this is not the case for the ICTA blend, where the exciton band is present (see panel g), consistent with the idea that this blend contains relatively small but pure polymer and fullerene domains, where excitons have to diffuse over a certain distance in order to become separated at the donor:acceptor interface (panel h). Figure S5c shows the exciton decay kinetics of the PBTTT:ICTA blend, from where an average lifetime of τ = 2.0 ± 0.4 ps for exciton dissociation was obtained from a triexponential fit (details of the fit are shown in Table S4). This suggests that, despite the inability of ICTA to intercalate and form a co-crystal with PBTTT, the size of the pure polymer domains in its blend is fairly small. In agreement with this interpretation, the polaron photoinduced absorption shows a rise on a similar time scale, which corresponds to a fraction of polaron pairs that are generated after exciton diffusion from pure polymer areas to the interface, (see Figure 4h), also consistent with the steady-state PL measurements (Figure S5). This rise is noticeably slower than that for the intercalated system, thus emphasizing the morphological differences of the blends (see section 4 in the SI).

Now we discuss the decay dynamics of the photogenerated charges in the blends and devices. Only the composite blend shows clear intensity-dependent decays, which start at ~10 ps and exhibit a half-time of ~4 ns at the highest intensity studied. This intensity-dependent behavior is also present in the total charge density on the ns time scale measured with TDCF, where a much faster decay is observed when the pulse intensity is increased by a factor of 10. From the fits of these decays (not shown), a predominant second-order kinetics can be obtained.

The scenario is completely different for the intercalated and nonintercalated systems. In the first case, a fast intensity-independent decay of the polaron absorption is observed. This decay can be fitted to a multiexponential decay with an average time constant of τ = 220 ± 20 ps (see Table S4). After ~2 ns, 80% of the charges are lost to this fast charge recombination, in agreement with other studies.[22,42,44,45] The TDCF data also show an intensity-independent first-order recombination process, in agreement with ns-TAS measurements by Laquai et al.[22] Our external quantum efficiency (EQE) measurements

DOI: 10.1021/acs.jpclett.7b01571
J. Phys. Chem. Lett. 2017, 8, 4061−4068

in the near-IR (see Figure S7) show a band at ~980 nm, which suggests that there are bound species with absorption coupled to the ground state that can generate free charges. These species therefore correspond to CT states. We envision that recombination of the most tightly bound states results in fast geminate recombination that starts from early times, leaving the loosely bound polaron pairs to survive recombination at longer time scales and being more prone to separation and extraction by a sufficiently large bias.

For the nonintercalated system, for which our simulations predict efficient free charge generation, the polaron TAS decays are surprisingly intensity-independent; however, they undergo an exponential decay with a much larger time constant (τ = 1.43 ± 0.08 ns) compared with the fully intercalated system. Importantly, charge recombination follows first-order decay also in TDCF, while charge extraction is rather slow; notice that charges are extracted only after ~100 ns (see n_{pre} in blue triangles in Figures S8e and S8f). Another important observation is the lack of near-IR absorption in our EQE measurements (see Figure S7) indicating that if there are bound species, their concentration is small and/or their coupling to the ground state is weak. Altogether, this evidences a scenario where charge pairs created at the donor:acceptor interface, after exciton dissociation, separate rapidly, thereby lowering their free energy (see Figure 2); however, only a few of these pairs split further to become fully independent charge carriers able to reach the electrodes. This suggests that the charges might remain morphologically confined in small polymer or fullerene domains. Alternatively, given the broad density of states distribution and a low electron mobility of higher adduct fullerenes, electrons may become readily trapped, preventing efficient charge extraction in the device.[37,47] Both scenarios are plausible, and it is likely that combination of both is responsible for the low efficiencies of free charge formation and predominant first-order recombination in this device; however, the exact mechanism is beyond the scope of this contribution.

This study reveals important differences in the charge carrier dynamics of PBTTT:fullerene blends depending on the heterojunction morphology and domain purity. For the 1:1 PBTTT:$PC_{70}BM$ blend with an intercalated morphology, our simulations and TDCF data show free carrier formation to proceed through a (Coulombically) bound precursor. However, as there are no internal domain boundaries, carriers can be efficiently extracted to the outside circuit with the assistance of an electric field. In agreement with this picture, geminate, first-order polaron recombination dominates the kinetics in the absence of an electric field (as observed in TAS or TDCF near V_{OC}), but there is a noticeable increase of the EGE when reversing the bias, thus rendering a strong voltage-dependent photocurrent. These observations are consistent with a recent semiempirical theoretical study of the effect of intermixed regions upon charge recombination.[27] In contrast, in the nonintercalated 1:1 PBTTT:ICTA system, there is a shallow energetic barrier to separate the interfacial CT state, and yet, most of the photogenerated charge carriers are either morphologically bound or energetically trapped charges in a more disordered blend.[37] As a consequence, polaron recombination as obtained by TAS is first-order, and the EGE remains at a low level independent of the applied voltage. An additional factor that can contribute to the poor charge separation and collection in the nonintercalated device may originate from the expected lower charge mobility of ICTA, as compared to $PC_{70}BM$,[48] which can hinder efficient charge generation and collection.[11]

It is only in the 1:4 PBTT:$PC_{70}BM$ system with a composite morphology that the majority of photogenerated polarons fully separate, then exhibiting slow, second-order recombination dynamics and an overall higher EGE. We propose that in this system charge separation benefits from the presence of larger and well-interconnected fullerene domains. It is also plausible that an energy cascade effect operates in the junction between the co-crystal and the semicrystallized $PC_{70}BM$ areas with higher electron affinity.[12,49] This is an effect unlikely to be present in the ICTA blends due to their small and noncrystallized domains, as can be observed in the WAXD data, which does not show the characteristic peak at q = 1.37 $Å^{-1}$, proposed to come from aggregated fullerene areas.[50,51] Note that this peak is only present for the composite blend where larger $PC_{70}BM$ domains are present.[30,31]

A second important conclusion comes from the direct comparison of TAS and TDCF data in Scheme 1. Here, by assuming that the two measurements overlap at ~6 ns and low excitation intensities (2.2 μJ cm^{-2}), we can obtain the polymer (hole) polaron extinction coefficient ε_P from the TAS data at the polaron maximum absorption. Using this approach, we estimate that $\varepsilon_P = (4.0 \pm 0.7) \times 10^4$ M^{-1} cm^{-1} for PBTTT hole polarons, which is consistent with published data for other polymers used in OPV.[52,53] We notice, however, that this value was obtained using only the 1:1 and 1:4 PBTTT:$PC_{70}BM$ transients. Interestingly, for the nonintercalated system, the optical and optoelectronical methods do not seem to agree in the charge density obtained; the extractable charge density determined by TDCF is ~2.6 times lower than the total charge in the blend, as estimated by TAS measurements. This is consistent with the idea that most of these charges are either morphologically or energetically trapped, rendering them vulnerable for geminate recombination and thus difficult to extract efficiently even under the influence of a strong bias. This is explicitly illustrated in the right panel of Scheme 1.

Finally, it is worth noticing in Scheme 1 that "instantaneous" (≤200 fs) charge generation is actually more efficient in the 1:1

Scheme 1. Absolute Polaron Density Kinetics from TAS (lines) on Thin Films and TDCF (open squares) on the Corresponding Devices for the Three Studied Systems Using Pulse Excitations at 540 nm and 2.2 μJ/cm^2[a]

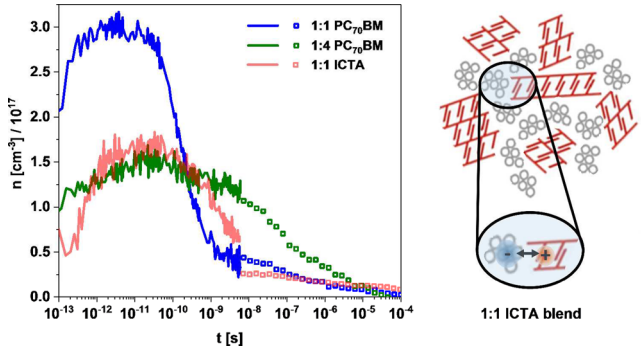

[a]A hole polaron extinction coefficient of (4.0 ± 0.7) × 10^4 M^{-1} cm^{-1} is obtained. The depiction at the right illustrates the proposed morphology that is believed to be present in the 1:1 PBTTT:ICTA, nonintercalated blend and is responsible for the discrepancy observed from TAS and TDCF (see text).

DOI: 10.1021/acs.jpclett.7b01571
J. Phys. Chem. Lett. 2017, 8, 4061−4068

PBTTT:$PC_{70}BM$ system, where in the range from ~200 fs to 45 ps polaron density is almost twice as high as that for the other two systems. However, notice that charge generation as determined by TAS does not discriminate between bound or free charges, and after ~200 ps the charge density in the other two blends is higher due to their slower charge recombination. While it is important to understand the polaron pair kinetics from the ultrafast time scales, it is the free charge density at times relevant for charge extraction that is mostly relevant to device operation.

We have demonstrated the impact of the interface morphology upon charge generation, recombination, and extraction in a combined kinetic study in blends and devices. While thermodynamic simulations show that charge separation is more efficient at an abrupt interface compared to an intercalated one, the former displays the lowest device efficiency. This is due to the inability of the nonintercalated system to form fully independent free charges in high-mobility domains that favor efficient extraction. Remarkably, in both extreme cases, where either intercalated or phase-separated domains predominate, charges undergo geminate recombination of bound polaron pairs. In stark contrast, the composite 1:4 PBTTT:$PC_{70}BM$ system is the only one that results in good extraction and delayed, nongeminate recombination. This indicates that both intermixed and pure phases are required for an efficient device.

METHODS

Film Preparation. For optical measurements (fs-TAS, steady-state PL) and device fabrication, solutions of PBTTT and $PC_{70}BM$ (or ICTA) in *ortho*-dichlorobenzene (ODCB) were prepared at a concentration between 15 and 30 mg mL^{-1}. The solutions were stirred and heated at 90 °C for at least 8 h to ensure full dissolution. The films were spun on cleaned glass substrates for 1 min at 1500 rpm. For WAXD measurements, films were prepared by drop-casting 30 mg mL^{-1} solutions of the neat polymer or the polymer/acceptor mixtures onto clean glass substrates.

Wide-Angle X-ray Diffraction (WAXD). The measurements were taken with a PANALYTICAL X'PERT-PRO Materials Research diffractometer (MRD) equipped with a nickel-filtered Cu $K\alpha_1$ beam, with λ = 1.54 Å and an X'CELERATOR detector. A current of I = 40 mA and an accelerating voltage of U = 40 kV were used. Data were corrected to account for different film the thicknesses, and the baseline was subtracted.

Device Fabrication. Precleaned, patterned indium tin oxide (ITO) substrates (15 Ω per square) were used and treated with oxygen plasma. On top of the ITO substrates, PEDOT:PSS was spun at 2500 rpm and dried on a hot plate at 150 °C in air for 30 min. Active layers for devices were prepared in a similar fashion as for the films used for optical measurements. Following, a counter electrode of calcium (10 nm) and aluminum (100 nm) was deposited by vacuum evaporation at 3 × 10^{-7} mbar. The active area of the devices used for TDCF was 0.01 cm^2. Devices were encapsulated with blue fix glue.

Transient Absorption Spectroscopy (TAS). Measurements were carried out with a commercial setup that comprises a 1 kHz Solstice (Newport Corporation) Ti:sapphire regenerative amplifier with 800 nm, 90 fs pulses. The output was passed through a beam splitter to generate the pump and probe pulses. The tunable pump pulse was generated in a TOPAS-Prime (light conversion) optical parametric amplifier and used to excite the sample with energies between 2 and 30 μJ cm^{-2} at 540 nm. The probe light was used to generate a near-IR continuum (800−1400 nm) in a sapphire crystal. A HELIOS transient absorption spectrometer (Ultrafast Systems) was used to collect transient absorption spectra and decays up to 6 ns. The time resolution of this setup was 200 fs. The films were kept at all times under a nitrogen atmosphere.

Time-Delayed Collection Field (TDCF). An optical pulse train generated by a diode-pumped, Q-switched Nd:YAG laser (NT242, EKSPLA, 500 Hz repetition rate, 3.8 ns pulse duration) was used to excite the sample. In the meantime, the device was held at a constant "prebias" set by an Agilent 81150 A pulse generator trough a home-built amplifier and then switched to a strong reverse bias "collection bias" after a certain delay time. The current through the device was measured via a grounded 10 Ω resistor in series with the sample and recorded with an Agilent DSO9104H oscilloscope. To compensate for the internal latency of the pulse generator, the laser pulse was delayed and homogeneously scattered in an 85 m long silica fiber (LEONI).

ASSOCIATED CONTENT

Supporting Information

The Supporting Information is available free of charge on the ACS Publications website at DOI: 10.1021/acs.jpclett.7b01571.

Structures of the donor polymer and fullerene acceptors as well as UV−vis steady-state absorption of the respective neat and blend films, details of the thermodynamic simulations and optical spectroscopy (TAS and PL) complementary data, EQE and device efficiency figures, and TDCF transient of devices (PDF)

AUTHOR INFORMATION

Corresponding Authors

*E-mail: neher@uni-potsdam.de (D.N.).
*E-mail: j.durrant@ic.ac.uk (J.R.D.).

ORCID

Elisa Collado-Fregoso: 0000-0002-2870-6983
Safa Shoaee: 0000-0001-8386-2893
Bob C. Schroeder: 0000-0002-9793-631X
Iain McCulloch: 0000-0002-6340-7217
James R. Durrant: 0000-0001-8353-7345

Notes

The authors declare no competing financial interest.

ACKNOWLEDGMENTS

This work was funded by UNVEiL, a BMBF project, the EPSRC (EP/IO1927B/1, EP/M023532/1, and EP/K011987/1), and the Welsh Assembly Government Sêr Cymru programme. E.C.-F. thanks CONACyT (scholarship 309929) and the Kernahan Fund from Imperial College London for funding. S.N.H. and I.K. were supported by the Westpac Bicentennial Foundation and by the Australian Research Council through a Discovery Early Career Researcher Award (DE140100433) and through the Centre of Excellence for Engineered Quantum Systems (CE110001013).

REFERENCES

(1) Gao, F.; Inganas, O. Charge Generation in Polymer−fullerene Bulk-Heterojunction Solar Cells. *Phys. Chem. Chem. Phys.* **2014**, *16*, 20291−20304.

DOI: 10.1021/acs.jpclett.7b01571
J. Phys. Chem. Lett. 2017, 8, 4061−4068

(2) Few, S.; Frost, M.; Nelson, J. Models of Charge Pair Generation in Organic Solar Cells. *Phys. Chem. Chem. Phys.* **2015**, *17*, 2311−2325.
(3) Bässler, H.; Köhler, A. Hot or Cold": How Do Charge Transfer States at the Donor−acceptor Interface of an Organic Solar Cell Dissociate? *Phys. Chem. Chem. Phys.* **2015**, *17*, 28451−28462.
(4) Dimitrov, S. D.; Durrant, J. R. Materials Design Considerations for Charge Generation in Organic Solar Cells. *Chem. Mater.* **2014**, *26*, 616−630.
(5) Vandewal, K.; Albrecht, S.; Hoke, E. T.; Graham, K. R.; Widmer, J.; Douglas, J. D.; Schubert, M.; Mateker, W. R.; Bloking, J. T.; Burkhard, G. F.; et al. Charge-Transfer States at Organic Interfaces. *Nat. Mater.* **2013**, *13*, 63−68.
(6) Bakulin, A. a; Rao, A.; Pavelyev, V. G.; van Loosdrecht, P. H. M.; Pshenichnikov, M. S.; Niedzialek, D.; Cornil, J.; Beljonne, D.; Friend, R. H. The Role of Driving Energy and Delocalized States for Charge Separation in Organic Semiconductors. *Science* **2012**, *335*, 1340−1344.
(7) Savoie, B. M.; Rao, A.; Bakulin, A. A.; Gelinas, S.; Movaghar, B.; Friend, R. H.; Marks, T. J.; Ratner, M. A. Unequal Partnership: Asymmetric Roles of Polymeric Donor and Fullerene Acceptor in Generating Free Charge. *J. Am. Chem. Soc.* **2014**, *136*, 2876−2884.
(8) Niedzialek, D.; Duchemin, I.; de Queiroz, T. B.; Osella, S.; Rao, A.; Friend, R.; Blase, X.; Kümmel, S.; Beljonne, D. First Principles Calculations of Charge Transfer Excitations in Polymer-Fullerene Complexes: Influence of Excess Energy. *Adv. Funct. Mater.* **2015**, *25*, 1972−1984.
(9) Jones, M. L.; Dyer, R.; Clarke, N.; Groves, C. Are Hot Charge Transfer States the Primary Cause of Efficient Free-Charge Generation in Polymer:fullerene Organic Photovoltaic Devices? A Kinetic Monte Carlo Study. *Phys. Chem. Chem. Phys.* **2014**, *16*, 20310−20320.
(10) Bernardo, B.; Cheyns, D.; Verreet, B.; Schaller, R. D.; Rand, B. P.; Giebink, N. C. Delocalization and Dielectric Screening of Charge Transfer States in Organic Photovoltaic Cells. *Nat. Commun.* **2014**, *5*, 3245.
(11) Philippa, B.; Stolterfoht, M.; Burn, P. L.; Juška, G.; Meredith, P.; White, R. D.; Pivrikas, A. The Impact of Hot Charge Carrier Mobility on Photocurrent Losses in Polymer-Based Solar Cells. *Sci. Rep.* **2015**, *4*, 5695.
(12) Jamieson, F. C.; Domingo, E. B.; McCarthy-Ward, T.; Heeney, M.; Stingelin, N.; Durrant, J. R. Fullerene Crystallisation as a Key Driver of Charge Separation in Polymer/fullerene Bulk Heterojunction Solar Cells. *Chem. Sci.* **2012**, *3*, 485.
(13) Shoaee, S.; Subramaniyan, S.; Xin, H.; Keiderling, C.; Tuladhar, P. S.; Jamieson, F.; Jenekhe, S. A.; Durrant, J. R. Charge Photogeneration for a Series of Thiazolo-Thiazole Donor Polymers Blended with the Fullerene Electron Acceptors PCBM and ICBA. *Adv. Funct. Mater.* **2013**, *23*, 3286−3298.
(14) Ma, W.; Tumbleston, J. R.; Wang, M.; Gann, E.; Huang, F.; Ade, H. Domain Purity, Miscibility, and Molecular Orientation at Donor/acceptor Interfaces in High Performance Organic Solar Cells: Paths to Further Improvement. *Adv. Energy Mater.* **2013**, *3*, 864−872.
(15) Vandewal, K.; Himmelberger, S.; Salleo, A. Structural Factors That Affect the Performance of Organic Bulk Heterojunction Solar Cells. *Macromolecules* **2013**, *46*, 6379−6387.
(16) Mukherjee, S.; Proctor, C. M.; Bazan, G. C.; Nguyen, T.; Ade, H. Significance of Average Domain Purity and Mixed Domains on the Photovoltaic Performance of High-Effi Ciency Solution-Processed Small-Molecule BHJ Solar Cells. *Adv. Energy Mater.* **2015**, *5*, 1500877.
(17) Mukherjee, S.; Jiao, X.; Ade, H. Charge Creation and Recombination in Multi-Length Scale Polymer:Fullerene BHJ. Solar Cell Morphologies. *Adv. Energy Mater.* **2016**, *6*, 1600699.
(18) Jiao, X.; Ye, L.; Ade, H. Quantitative Morphology-Performance Correlations in Organic Solar Cells: Insights from Soft X-Ray Scattering. *Adv. Energy Mater.* **2017**, 1700084.
(19) Tumbleston, J. R.; Collins, B. a.; Yang, L.; Stuart, A. C.; Gann, E.; Ma, W.; You, W.; Ade, H. The Influence of Molecular Orientation on Organic Bulk Heterojunction Solar Cells. *Nat. Photonics* **2014**, *8*, 385−391.
(20) Ryno, S. M.; Fu, Y. T.; Risko, C.; Bredas, J. L. Polarization Energies at Organic-Organic Interfaces: Impact on the Charge Separation Barrier at Donor-Acceptor Interfaces in Organic Solar Cells. *ACS Appl. Mater. Interfaces* **2016**, *8*, 15524−15534.
(21) Kästner, C.; Egbe, D. A. M.; Hoppe, H. Polymer Aggregation Control in Polymer−fullerene Bulk Heterojunctions Adapted from Solution. *J. Mater. Chem. A* **2015**, *3*, 395−403.
(22) Gehrig, D. W.; Howard, I. A.; Sweetnam, S.; Burke, T. M.; Mcgehee, M. D.; Laquai, F. The Impact of Donor − Acceptor Phase Separation on the Charge Carrier Dynamics in pBTTT:PCBM Photovoltaic Blends. *Macromol. Rapid Commun.* **2015**, *36*, 1054−1060.
(23) Yan, H.; Song, Y.; McKeown, G. R.; Scholes, G. D.; Seferos, D. S. Adding Amorphous Content to Highly Crystalline Polymer Nanowire Solar Cells Increases Performance. *Adv. Mater.* **2015**, *27*, 3484−3491.
(24) Collado-Fregoso, E.; Deledalle, F.; Utzat, H.; Tuladhar, P. S.; Dimitrov, S. D.; Gillett, A.; Tan, C. H.; Zhang, W.; McCulloch, I.; Durrant, J. R. Photophysical Study of DPPTT-T/PC70BM Blends and Solar Devices as a Function of Fullerene Loading: An Insight into EQE Limitations of DPP-Based Polymers. *Adv. Funct. Mater.* **2017**, *27*, 1604426.
(25) Utzat, H.; Dimitrov, S. D.; Wheeler, S.; Collado-Fregoso, E.; Tuladhar, P. S.; Schroeder, B. C.; McCulloch, I.; Durrant, J. R. Charge Separation in Intermixed Polymer:PC70BM Photovoltaic Blends: Correlating Structural and Photophysical Length Scales as a Function of Blend Composition. *J. Phys. Chem. C* **2017**, *121*, 9790−9801.
(26) Lyons, B. P.; Clarke, N.; Groves, C. The Relative Importance of Domain Size, Domain Purity and Domain Interfaces to the Performance of Bulk-Heterojunction Organic Photovoltaics. *Energy Environ. Sci.* **2012**, *5*, 7657.
(27) Finck, B. Y.; Schwartz, B. J. Drift-Diffusion Studies of Compositional Morphology in Bulk Heterojunctions: The Role of the Mixed Phase in Photovoltaic Performance. *Phys. Rev. Appl.* **2016**, *6*, 1−16.
(28) Miller, N. C.; Sweetnam, S.; Hoke, E. T.; Gysel, R.; Miller, C. E.; Bartelt, J. A.; Xie, X.; Toney, M. F.; McGehee, M. D. Molecular Packing and Solar Cell Performance in Blends of Polymers with a Bisadduct Fullerene. *Nano Lett.* **2012**, *12*, 1566−1570.
(29) Miller, N. C.; Cho, E.; Gysel, R.; Risko, C.; Coropceanu, V.; Miller, C. E.; Sweetnam, S.; Sellinger, A.; Heeney, M.; McCulloch, I.; et al. Factors Governing Intercalation of Fullerenes and Other Small Molecules between the Side Chains of Semiconducting Polymers Used in Solar Cells. *Adv. Energy Mater.* **2012**, *2*, 1208−1217.
(30) Miller, N. C.; Cho, E.; Junk, M. J. N.; Gysel, R.; Risko, C.; Kim, D.; Sweetnam, S.; Miller, C. E.; Richter, L. J.; Kline, R. J.; et al. Use of X-Ray Diffraction, Molecular Simulations, and Spectroscopy to Determine the Molecular Packing in a Polymer-Fullerene Bimolecular Crystal. *Adv. Mater.* **2012**, *24*, 6071−6079.
(31) Buchaca-Domingo, E.; Ferguson, a. J.; Jamieson, F. C.; McCarthy-Ward, T.; Shoaee, S.; Tumbleston, J. R.; Reid, O. G.; Yu, L.; Madec, M.-B.; Pfannmöller, M.; et al. Additive-Assisted Supramolecular Manipulation of Polymer:fullerene Blend Phase Morphologies and Its Influence on Photophysical Processes. *Mater. Horiz.* **2014**, *1*, 270.
(32) Wade, J.; Wood, S.; Collado-Fregoso, E.; Heeney, M.; Durrant, J. R.; Kim, J.-S. Impact of Fullerene Intercalation on Structural and Thermal Properties of Organic Photovoltaic Blends. *J. Phys. Chem. C* **2017**, Submitted.
(33) Hood, S. N.; Kassal, I. Entropy and Disorder Enable Charge Separation in Organic Solar Cells. *J. Phys. Chem. Lett.* **2016**, *7*, 4495−4500.
(34) Clarke, T. M.; Durrant, J. R. Charge Photogeneration in Organic Solar Cells. *Chem. Rev.* **2010**, *110*, 6736−6767.
(35) Gregg, B. A. Entropy of Charge Separation in Organic Photovoltaic Cells: The Benefit of Higher Dimensionality. *J. Phys. Chem. Lett.* **2011**, *2*, 3013−3015.
(36) Poelking, C.; Cho, E.; Malafeev, A.; Ivanov, V.; Kremer, K.; Risko, C.; Brédas, J. L.; Andrienko, D. Characterization of Charge-Carrier Transport in Semicrystalline Polymers: Electronic Couplings, Site Energies, and Charge-Carrier Dynamics in Poly(bithiophene-Alt-Thienothiophene) [PBTTT]. *J. Phys. Chem. C* **2013**, *117*, 1633−1640.

DOI: 10.1021/acs.jpclett.7b01571
J. Phys. Chem. Lett. 2017, 8, 4061−4068

(37) Nyman, M.; Sandberg, O. J.; Österbacka, R. Charge Transport in Intercalated and Non-Intercalated Polymer:fullerene Blends. *Synth. Met.* **2015**, *201*, 6−10.
(38) Kniepert, J.; Schubert, M.; Blakesley, J.; Neher, D. Photogeneration and Recombination in P3HT: PCBM Solar Cells Probed by Time Delayed Collection Field Experiments. *J. Phys. Chem. Lett.* **2011**, *2*, 700−705.
(39) Kurpiers, J.; Neher, D. Dispersive Non-Geminate Recombination in an Amorphous Polymer:Fullerene Blend. *Sci. Rep.* **2016**, *6*, 26832.
(40) Zusan, A.; Vandewal, K.; Allendorf, B.; Hansen, N. H.; Pflaum, J.; Salleo, A.; Dyakonov, V.; Deibel, C. The Crucial Influence of Fullerene Phases on Photogeneration in Organic Bulk Heterojunction Solar Cells. *Adv. Energy Mater.* **2014**, *4*, 1400922.
(41) Rance, W. L.; Ferguson, A. J.; McCarthy-Ward, T.; Heeney, M.; Ginley, D. S.; Olson, D. C.; Rumbles, G.; Kopidakis, N. Photoinduced Carrier Generation and Decay Dynamics in Intercalated and Non-Intercalated Polymer:fullerene Bulk Heterojunctions. *ACS Nano* **2011**, *5*, 5635−5646.
(42) Scarongella, M.; Paraecattil, A. A.; Buchaca-Domingo, E.; Douglas, J. D.; Beaupré, S.; McCarthy-Ward, T.; Heeney, M.; Moser, J.-E.; Leclerc, M.; Fréchet, J. M. J.; et al. The Influence of Microstructure on Charge Separation Dynamics in Organic Bulk Heterojunction Materials for Solar Cell Applications. *J. Mater. Chem. A* **2014**, *2*, 6218−6230.
(43) Dou, F.; Buchaca-Domingo, E.; Sakowicz, M.; Rezasoltani, E.; McCarthy-Ward, T.; Heeney, M.; Zhang, X.; Stingelin, N.; Silva, C. The Effect of Phase Morphology on the Nature of Long-Lived Charges in Semiconductor Polymer:fullerene Systems. *J. Mater. Chem. C* **2015**, *3*, 3722−3729.
(44) Scarongella, M.; De Jonghe-Risse, J.; Buchaca-Domingo, E.; Causa', M.; Fei, Z.; Heeney, M.; Moser, J. E.; Stingelin, N.; Banerji, N. A Close Look at Charge Generation in Polymer: Fullerene Blends with Microstructure Control. *J. Am. Chem. Soc.* **2015**, *137*, 2908−2918.
(45) Causa', M.; De Jonghe-Risse, J.; Scarongella, M.; Brauer, J. C.; Buchaca-Domingo, E.; Moser, J.-E.; Stingelin, N.; Banerji, N. The Fate of Electron−Hole Pairs in Polymer:Fullerene Blends for Organic Photovoltaics. *Nat. Commun.* **2016**, *7*, 12556.
(46) Dimitrov, S.; Schroeder, B.; Nielsen, C.; Bronstein, H.; Fei, Z.; McCulloch, I.; Heeney, M.; Durrant, J. Singlet Exciton Lifetimes in Conjugated Polymer Films for Organic Solar Cells. *Polymers* **2016**, *8*, 14.
(47) Lenes, M.; Shelton, S. W.; Sieval, A. B.; Kronholm, D. F.; Hummelen, J. C.; Blom, P. W. M. Electron Trapping in Higher Adduct Fullerene-Based Solar Cells. *Adv. Funct. Mater.* **2009**, *19*, 3002−3007.
(48) Faist, M. A.; Shoaee, S.; Tuladhar, S.; Dibb, G. F. A.; Foster, S.; Gong, W.; Kirchartz, T.; Bradley, D. D. C.; Durrant, J. R.; Nelson, J. Understanding the Reduced Efficiencies of Organic Solar Cells Employing Fullerene Multiadducts as Acceptors. *Adv. Energy Mater.* **2013**, *3*, 744−752.
(49) Groves, C. Suppression of Geminate Charge Recombination in Organic Photovoltaic Devices with a Cascaded Energy Heterojunction. *Energy Environ. Sci.* **2013**, *6*, 1546.
(50) Piersimoni, F.; Chambon, S.; Vandewal, K.; Mens, R.; Boonen, T.; Gadisa, A.; Izquierdo, M.; Filippone, S.; Ruttens, B.; D'haen, J.; Martin, N.; Lutsen, L.; Vanderzande, D.; Adriaensens, P.; Manca, J. V. Influence of Fullerene Ordering on the Energy of the Charge-Transfer State and Open-Circuit Voltage in Polymer:fullerene Solar Cells. *J. Phys. Chem. C* **2011**, *115*, 10873−10880.
(51) Tumbleston, J. R.; Yang, L.; You, W.; Ade, H. Morphology Linked to Miscibility in Highly Amorphous Semi-Conducting Polymer/fullerene Blends. *Polymer* **2014**, *55*, 4884−4889.
(52) Shuttle, C. G.; O'Regan, B.; Ballantyne, A. M.; Nelson, J.; Bradley, D. D. C.; Durrant, J. R. Bimolecular Recombination Losses in Polythiophene: Fullerene Solar Cells. *Phys. Rev. B: Condens. Matter Mater. Phys.* **2008**, *78*, 1−4.
(53) Tautz, R.; Da Como, E.; Limmer, T.; Feldmann, J.; Egelhaaf, H.-J.; von Hauff, E.; Lemaur, V.; Beljonne, D.; Yilmaz, S.; Dumsch, I.; Allard, S.; Scherf, U. Structural Correlations in the Generation of Polaron Pairs in Low-Bandgap Polymers for Photovoltaics. *Nat. Commun.* **2012**, *3*, 970.

DOI: 10.1021/acs.jpclett.7b01571
J. Phys. Chem. Lett. 2017, 8, 4061−4068